Cancer Nanotechnology

RESEARCH Open Access

Nanocomplex hyaluronic acid/ganciclovir@ZIF-8 for ganciclovir efficient delivery and targeted anti-KSHV treatment

Fangling Li[1,2†], Chengjing Liu[1†], Wenyi Gu[3], Qianhe Xu[4], Dongmei Li[1*], Dongdong Cao[1*] and Zhiyong Liu[2*]

†Fangling Li and Chengjing Liu have contributed equally to this work.

*Correspondence: lidong_abc@126.com; caodongd2023@sina.com; lzyongclin@sina.com

[1] School of Medicine, Key Laboratory of Xinjiang Endemic and Ethnic Diseases/International Science and Technology Cooperation Base of Xinjiang Endemic and Ethnic Diseases, Shihezi University, Shihezi 832002, People's Republic of China
[2] School of Chemistry and Chemical Engineering, Shihezi University, Shihezi 832003, People's Republic of China
[3] Australian Institute for Bioengineering and Nanotechnology (AIBN), University of Queensland (UQ), Corner College and Cooper Roads, Building 75, Brisbane, QLD 4072, Australia
[4] School of Chemistry and Molecular Engineering, East China University of Science and Technology, Shanghai 200237, People's Republic of China

Abstract

Kaposi's sarcoma-associated herpesvirus (KSHV) infection can cause a variety of tumors and is one of the leading causes of death in acquired immune deficiency syndrome (AIDS) patients. As a small molecule antiviral drug, ganciclovir (GCV) can be used for anti-KSHV treatment. However, GCV has non-specific action and toxic side effects in vivo, and how to make it safer and more effective against KSHV is still a great challenge. By encapsulating GCV into metal–organic skeleton material zeolitic imidazolate framework-8 (ZIF-8) and further modification of hyaluronic acid (HA), the nanomedical delivery system of GCV (HA/GCV@ZIF-8) has been developed for efficient GCV delivery and targeted anti-KSHV treatment. The modification of HA leads to the targeted binding of the nanocomplex with the overexpressed CD44 receptors in tumor cell membranes, resulting in the increased accumulation and cellular uptake of GCV. Exploiting the decomposition property of ZIF-8 under acidic conditions, the nanocomplex exhibits pH-responsive drug release in slightly acidic tumor environment. In addition, HA/GCV@ZIF-8 not only suppresses expression of KSHV pathogenic genes with less drug dose, but also inhibits the ability of cell proliferation and migration. In vivo anti-tumor results showed that HA/GCV@ZIF-8 accumulated in tumor cells and effectively inhibited tumor growth. The results open a gate for the targeted anti-KSHV treatment.

Keywords: Anti-KSHV treatment, Ganciclovir, Drug-carrying nanocomplex, pH-responsive drug release

Graphical Abstract

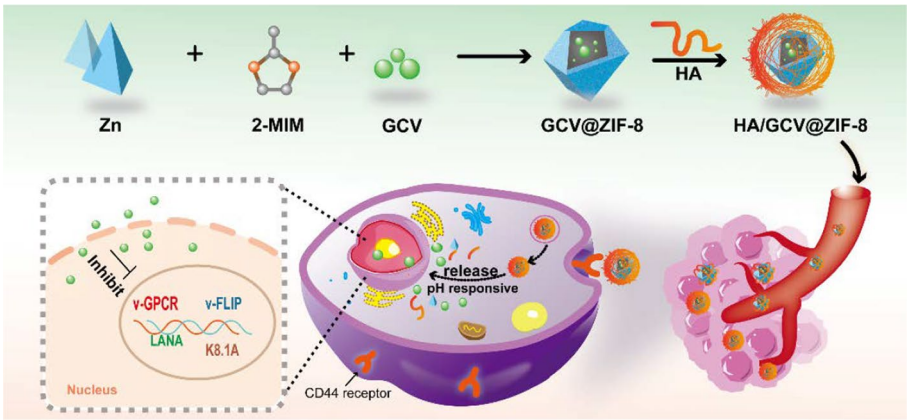

Introduction

Kaposi's sarcoma-associated herpesvirus (KSHV) is a carcinogenic virus belonging to the herpesvirus family (Ablashi et al. 2002; Schulz 2000). The virus can cause Kaposi's sarcoma (KS), which was the most common acquired immune deficiency syndrome (AIDS)-related malignancy (Journo et al. 2021). Patients with AIDS are susceptible to KSHV, widespread human immunodeficiency virus (HIV) infection has caused an epidemic of KS (Labo et al. 2015; Wu et al. 2022). It is very necessary to control the pathogenicity of KSHV.

At present, the main treatment methods of KS include surgery, radiation therapy and chemical therapy (Iftode et al. 2020; Carbone et al. 2022; Yang et al. 2024). However, these methods are mainly for the treatment of tumors, and are not direct anti-KSHV treatment. The surgical treatment for patients leads to great trauma, and the tumor metastasis would increase the risk and reduce the success rate of surgery (Ye et al. 2023). Radiation therapy is a kind of local treatment, which is easy to produce toxic and side effects on normal tissues and cause complications. Chemotherapy, including doxorubicin, vincristine, bleomycin and other drugs, has great toxicity and great pain to the patients (Krell and Stebbing 2014; Valantin et al. 2022; Chang and Ganem 2013; Delyon et al. 2019). The above therapeutic methods are symptomatic treatments for the tumor phenotype, but they are all indirect therapies, and cannot control the pathogeny KSHV and thereby cannot inhibit the root cause of tumorigenesis and development.

Currently, the main available treatment for anti-KSHV is the antiviral drugs, KSHV DNA polymerase inhibitors including ganciclovir, acyclovir and cidofovir (Chou 2021; Coen et al. 2014; Fang et al. 2022), which can act directly on the virus (Son et al. 2013; Chen et al. 2020). Ganciclovir (GCV) is a 2′-deoxyguanine nucleotide derivative that inhibits herpesvirus replication and is a broad-spectrum antiviral drug (Al-Badr and Ajarim 2018). GCV triphosphate can inhibit viral DNA synthesis in the following ways: first, it competes with guanosine triphosphate to inhibit viral DNA polymerase; second,

incorporation into the DNA of the virus and the host cells, resulting in the termination of viral DNA synthesis (Zhang et al. 2021; Märtson et al. 2022). Compared with other drugs, GCV was a widely used anti-KSHV drug in clinical practice. In KSHV-infected patients, GCV has been shown to effectively reduce the viral load of KSHV in peripheral blood (Morillo-Gutierrez et al. 2017) and reduce viral shedding in saliva (Casper et al. 2008). Although GCV can inhibit the DNA polymerase of KSHV, it still faces the trouble of being non-specific to the infection site and low transmembrane ability, which leads to many toxic side effects, such as various types of thrombocytopenia, persistent myelosuppression, liver and kidney damage (Al-Badr and Ajarim 2018; Ho et al. 2021; Qin et al. 2022). Therefore, it is a great clinical challenge to establish a GCV drug delivery system that can increase the concentration of GCV in target cells.

The rapid development of nanotechnology and its interaction with multiple disciplines have provided new ideas for the treatment of cancer (Merlin et al. 2023; Overchuk and Zheng 2018; Tao et al. 2021). Metal–organic skeleton materials have attracted wide attention in biomedical fields such as bioimaging, chemotherapy drug delivery, photothermal therapy and photodynamic therapy due to their clear structure, large pore size, specific surface area and adjustable skeleton (Jia et al. 2023; Ding et al. 2022; Wu and Yang 2017; Liu et al. 2023; Feng et al. 2019). Zeolite imidazole salt framework-8 (ZIF-8) is a biocompatible porous material constructed by the coordination of zinc ions and 2-methylimidazole (Jin and Shang 2021; Xie et al. 2022). ZIF-8 has a stable structure in a neutral physiological environment. In a slightly acidic tumor environment (pH = 4.5–6.5), the ligand 2-methylimidazole chain in ZIF-8 can be protonated, destroying the coordination between zinc ions and the imidazole ring, resulting in the gradual disintegration of the ZIF-8 structure and the release of drugs. This unique pH response disintegration property makes ZIF-8 a promising drug delivery vehicle (Shi et al. 2020; Ziqi et al. 2023; Lu et al. 2023). Hyaluronic acid (HA) can be found in extracellular tissues and plays an important role in many biological processes such as cell adhesion, growth, migration, and differentiation (Serra et al. 2023). The HA receptor CD44 is specifically overexpressed on a variety of tumor cells. Nanomedical drug delivery systems mediated by the ligand HA and the receptor CD44 actively target tumor sites which provide more options for the targeted delivery of a variety of drugs, and their good biocompatibility, biodegradability and non-immunogenicity have also received extensive attention (Luo et al. 2019; Kesharwani et al. 2022). Therefore, we envision to use nanomedicine delivery systems as an effective strategy to solve the problem of delivery GCV.

Aiming at the non-specific, toxic and low transmembrane capacity of GCV in the treatment of KSHV, we designed the nanomedical delivery system of GCV, nanocomplex HA/GCV@ZIF-8, by in situ encapsulation and ligand interaction for targeted delivery of GCV (Scheme 1). In vitro drug release experiments verified the pH response function of HA/GCV@ZIF-8. In vivo and in vitro fluorescence imaging demonstrated the targeting effect of drug-loaded nanocomplexes on KSHV infection sites. A series of cell experiments demonstrated the anti-KSHV effect of HA/GCV@ZIF-8 in vitro, and further tumor formation experiments in nude mice demonstrated its anti-tumor effect in vivo.

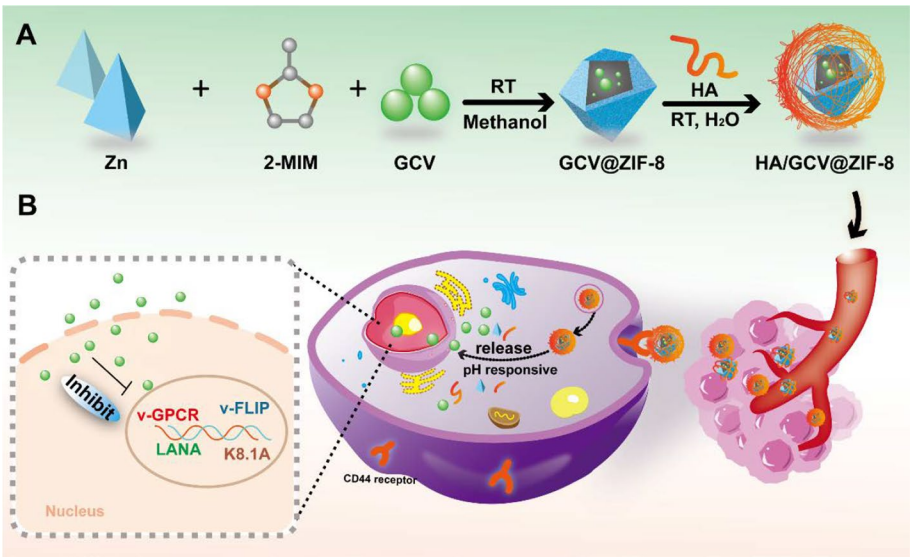

Scheme 1 Preparation of HA/GCV@ZIF-8 and schematic diagram of KSHV resistance

Materials and methods

Materials

Zinc nitrate hexahydrate ($Zn(NO_3)_2{\cdot}6H_2O$), 2-methylimidazole (2-MIM), hyaluronic acid (HA), new incyanine green (IR820), DMSO were obtained from Aladdin. GCV was obtained from Adamas.

Methods for preparing GCV@ZIF-8 and HA/GCV@ZIF-8

Dissolved GCV (100 mg) in DMSO (2 mL) for ultrasonic. Added $Zn(NO_3)_2{\cdot}6H_2O$ (240 mg) into 10 mL methanol, stirred and added 400 μL (20 mg) of GCV. And then added 2-MIM (480 mg in 10 mL methanol), stirring for 12 h, washed with 50% ethanol and centrifuged for 3 times. The centrifugation speed and time were 8000 rpm for 10 min, and finally put into a vacuum drying oven at 40 ℃. After drying for 12 h, the white solid product GCV@ZIF-8 was obtained.

The synthesis method of ZIF-8 is the same as above, except that GCV is not added.

HA (90 mg) was ultrasonically dissolved in 30 mL ultra-pure water, and then GCV@ZIF-8 (80 mg) was added to continue ultrasound until the mixture was uniform. After 24 h stirring at room temperature, ultra-pure water was washed and centrifuged for 3 times at 13,000 rpm for 10 min. Finally, the compound was freeze-dried in a freeze-drying machine for 24 h. The white solid product HA/GCV@ZIF-8 was obtained.

Structural characterization of HA/GCV@ZIF-8

The morphology of HA/GCV@ZIF-8 was observed by the transmission electron microscope (TEM, HT7700, Japan) and scanning electron microscope (SEM, SU8010, Japan). Nanoplus-3 was used to detect the particle size and Zeta potential. X-ray diffraction (XRD, Bruker D8 Advance, Germany), Fourier transform infrared spectrometer (FTIR, VERTEX 70, Bruker, USA) and thermogravimetric analyzer (HP-TGA 75),

the crystal structure, chemical structure and thermal stability of the product were tested.

Drug loading rate and release experiment in vitro

Dissolved HA/GCV@ZIF-8 (1 mg) in PBS solution (pH = 1), measured the absorbance value (OD_{252nm}), and tested the GCV mass through the standard curve (Figure S1). Finally, calculated the GCV loading rate (LD) of HA/GCV@ZIF-8 according to the following formula:

$$\mathrm{LD}\ (\%) = \frac{M_{GCV}}{M_{HA}} \times 100. \tag{1}$$

M_{GCV} the amount of encapsulated GCV, and M_{HA} the amount of HA/GCV@ZIF-8.

Dispersed HA/GCV@ZIF-8 (10 mg) in the PBS solution (pH = 7.4 and pH = 5.0) and transferred to the dialysis bag, then immersed in two PBS solutions (23 mL). Put them in a shaker (37 ℃, 100 rpm). Absorbed the supernatant (4 mL) at different times, and then added fresh PBS solution (4 mL). Measured the OD $value_{(252\ nm)}$ to calculate GCV release at each time point. The cumulative release rate of GCV (*Er*) as following:

$$Er(\%) = \frac{V_e \sum_1^{n-1} c_i + V_0 c_n}{M_{GCV}} \times 100. \tag{2}$$

M_{GCV} the amount of encapsulated GCV, V_e the volume per sample, c_i the concentration of GCV in the i th sample, V_0 the total volume of buffer, and c_n the concentration of GCV in the n th sample.

Hemolysis and stability test in vitro

ZIF-8, GCV@ZIF-8, HA/GCV@ZIF-8 (2 mg/mL) solutions were prepared with PBS solution. 0.1%Tritonx-100 and PBS were used as positive and negative group. Fresh sterile defibrillated sheep blood (3 mL) was absorbed with PBS (10 mL) solution at 2000 rpm, centrifuged 3 times for 10 min/time, and then discarded the supernatant, thus 5%(v/v) erythrocyte suspension was prepared, and then added into 0.1% Tritonx-100 and PBS to shake at 37 ℃, 100 rpm for 2 h, and then centrifugated at 2000 rpm for 10 min. The macroscopic hemolysis phenomenon of each group was recorded by taking photos, sucked the supernatant of each group was tomeasure the OD_{540nm} value. Hemolysis rate was shown as following (η):

$$\eta\% = \frac{OD_s - OD_{PBS}}{OD_t - OD_{PBS}} \times 100. \tag{3}$$

OD_s the sample group's OD value, OD_{PBS} the PBS group's OD value, and OD_t the 0.1%TritonX-100 group's OD value.

GCV@ZIF-8 and HA/GCV@ZIF-8 (1 mg/mL) were dissolved in 50% FBS, respectively, and added into 96-well plates, placed in a 37 ℃ incubator to measure the $OD_{(600\ nm)}$ values. The changes of OD value can be seen as the turbidity change of drug-carrying nanocomplex.

Cell culture and cytotoxicity

The SK-RG and KMM cells were KSHV-positive cells, and the origin and culture methods described in our previous study (Li et al. 2024). The cytotoxicity of ZIF-8, HA/ZIF-8, GCV@ZIF-8 and HA/GCV@ZIF-8 was detected by MTT assay. The cells were seed at a density of 2000 cells/peer well and incubated for 12 h. Replaced the supernatant with complete DMEM, and added into different concentrations of nanocomplex. After 48 h, MTT (20 μL, 5 mg/mL) was added and co-culture for another 4 h at 37 °C in the dark, then removed the supernatant and added the dimethyl sulfoxide (DMSO, 100 μL) to measure the OD value.

HA competition and cellular uptake experiment in vitro

Seeded the cells into 96-well plates at a density of 5000 cells per well, and then replaced with complete media after culture adhesion, and mixed solution of free HA, HA/GCV@ZIF-8. HA/GCV@ZIF-8 and free HA was added (the concentration of HA was 1 mg/mL) for 48 h to measure the OD value at 490 nm.

For observation, we loaded fluorescent dye new indocyanine green (IR820) into GCV@ZIF-8 and HA/GCV@ZIF-8. After cultured for 12 h in a 24-well plates (sterile cover slides were placed in each well), GCV@ZIF-8 and HA/GCV@ZIF-8 were added to co-culture for another 4 h, 4% paraformaldehyde was uesd to fix the KMM cells for 15 min and DAPI was uesd to stain for 10 min, 50% glycerin was sealed and observed by confocal laser microscope (CLSM).

Cell proliferation, migration and scratch experiments

After culturing with GCV@ZIF-8 and HA/GCV@ZIF-8 for 24 h. The cells were seeded into a 96-well plate and MTT solution was added from day 1 to day 3. A microplate reader was used to detect the ability of cell proliferation.

After treated with GCV@ZIF-8 and HA/GCV@ZIF-8 for 24 h, the KMM and SK-RG cells were collected and mixed in 150 μL of the pure DMEM (10,000 cells) and seeded in the upper chamber of a transwell plate, and 800 μL of DMEM with 10% serum in the lower chamber. After 36 h, the cells were fixed with paraformaldehyde for 20 min, and then stained with 0.1% crystal violet for 15 min.

After the drug-carrying nanocomplex treatment KMM and SK-RG cells for 4 h, use the 1 mL sterile pipette tip to streak a horizontal line at the bottom of the six-well plate, and than added into 2 mL of medium. After culture, the scratches at the same position were photographed at 0 h, 12 h, 24 h and 36 h.

RT-PCR

The extraction of RNA and synthesize of cDNA was accorded to the kit instructions (Takara, Japan). The method of real-time PCR was described in our previous study (Li et al. 2023) and the primer is shown in Table S1.

Tumor model building and in vivo fluorescence imaging

All animal experiments were conducted according to the protocol approved by the Institutional Animal Care and Use Committee of Shihezi University. The tumor model of

female nude mice was established by injecting KMM (3.0×10^8/mL, 150 μL) cells into the subcutaneously. The internal fluorescence of IR820 (2 mg/kg) was used to monitor the distribution of drug-carrying nanocomplex in vivo. When the volume of tumor is close to 200 mm^3, HA/GCV@ZIF-8 and GCV@ZIF-8 were injected the peritumoral. The nude mice were photographed with the small animal fluorescence and bioluminescence imaging system (Vieworks Smart-LF, Korea) at 1 h, 2.5 h, 8 h and 24 h. After killing, the tumor bodies and major organs were taken for photography.

In vivo anti-tumor experiment

The nude mouse tumor model was established. When the tumor volume close to 100 mm^3, divided nude mice into PBS, free GCV, ZIF-8, HA/ZIF-8, GCV@ZIF-8, and HA/GCV@ZIF groups randomly, and were treated with peritumoral injection every 4 days (GCV dose: 2.0 mg/kg). Tumor volume and body weight of nude mice were measured before each injection. After 21 days, the nude mice were killed and HE staining was performed on tumors and major organs.

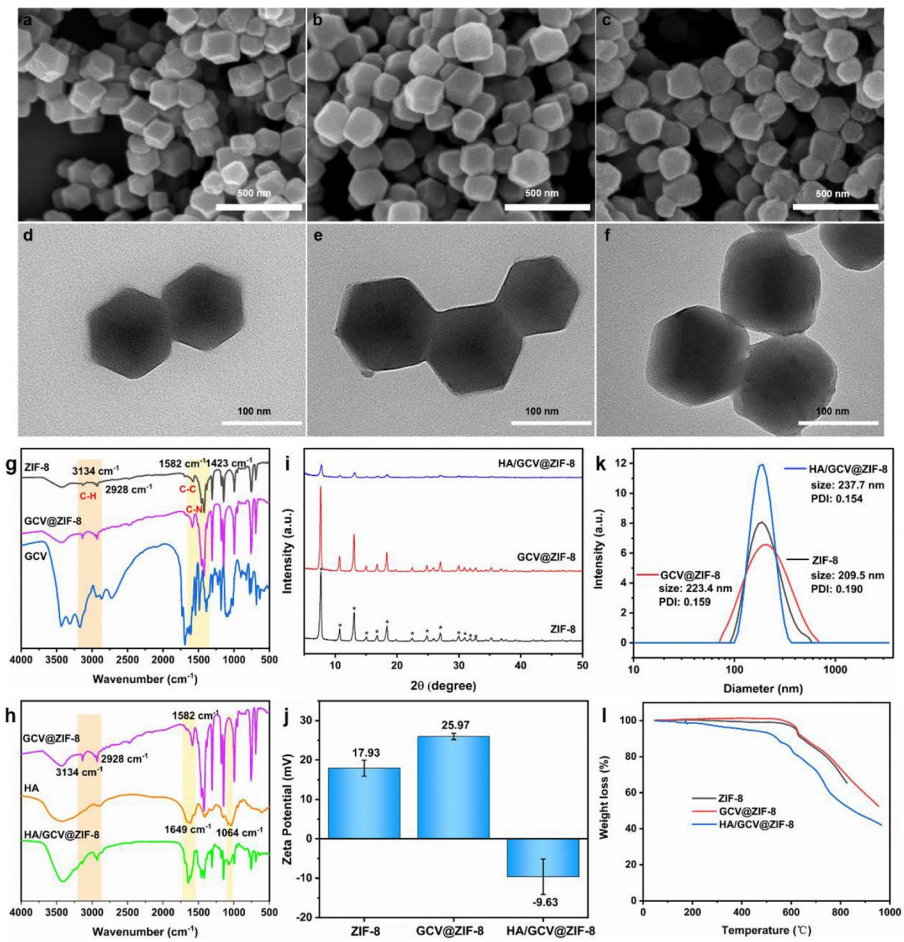

Fig. 1 Morphology and structural characterization of drug-carrying nanocomplex. **a**–**c** SEM images of ZIF-8, GCV@ZIF-8, HA/GCV@ZIF-8 and **d**–**f** TEM images, **g**, **h** infrared absorption spectra of ZIF-8, GCV@ZIF-8, HA/GCV@ZIF-8, **i** XRD, **j** Zeta potential, **k** particle size distribution, and **l** thermogravimetric curves. Data are presented as mean ± SD ($n = 3$)

Statistical analysis

SPSS 13.0 and Origin 2018 software were used to analyze the experimental data and $P < 0.05$ was considered statistically significant and the data were expressed as mean ± standard deviation.

Results and discussion

Preparation and characterization of GCV@ZIF-8, HA/GCV@ZIF-8

HA/GCV@ZIF-8 was prepared according to Scheme 1, and GCV was loaded into ZIF-8 by the in situ encapsulation. The morphologies of ZIF-8, GCV@ZIF-8 and HA/GCV@ZIF-8 were observed by SEM and TEM. As shown in Fig. 1a, b, ZIF-8 and GCV@ZIF-8 exhibit a dodecahedral structure. GCV@ZIF-8 further coated by HA, the angular edges of the dodecahedron become rounded and no longer exhibit a dodecahedral shape (Fig. 1c). At the same time, it is also obvious in the TEM of HA/GCV@ZIF-8 that the outer surface of GCV@ZIF-8 was coated with a film-like substance (Fig. 1d–f), indicating that HA was successfully coated on GCV@ZIF-8. In addition, it can be found that the dodecahedron shape does not change after loading GCV with ZIF-8.

To further verify whether GCV was encapsulated inside ZIF-8 and whether HA was successfully coated, we tested GCV, ZIF-8, GCV@ZIF-8, HA, HA/GCV@ZIF-8 using the infrared absorption spectroscopy. And found that the absorption spectrum of ZIF-8, 3134 cm^{-1} and 2928 cm^{-1} were C–H bond stretching vibration peaks on imidazole rings, 1582 cm^{-1} was C–C bond stretching vibration peaks, and 1432 cm^{-1} was C–N bond stretching vibration peaks. The infrared absorption peak of GCV@ZIF-8 was mainly characterized by the characteristic absorption peak of ZIF-8, which indicated that ZIF-8 had enclosed GCV (Fig. 1g). Therefore, there is basically no characteristic absorption peak of GCV in the absorption spectrum of GCV@ZIF-8. 1649 cm^{-1} and 1064 cm^{-1} were, respectively, the stretching vibration peaks of the C=O bond of HA and the stretching vibration peaks of C–OH (Fig. 1h). The infrared absorption peak of HA/GCV@ZIF-8 was composed of GCV@ZIF-8 and HA, which also indicated that HA was coated on GCV@ZIF-8.

XRD proved that the crystal structures of HA/GCV@ZIF-8, GCV@ZIF-8 and ZIF-8 were basically similar (Fig. 1i), which indicated that the crystallinity of ZIF-8 was not affected by the inclusion of GCV and HA. However, the diffraction peak intensity of HA/GCV@ZIF-8 decreases after HA modification, which may be due to the fact that the amorphous HA coated on GCV@ZIF-8 had a certain effect on the crystal structure. HA contains a large number of carboxyl groups, which can be coated on GCV@ZIF-8 through coordination interaction with Zn^{2+} in ZIF-8. The potential value of ZIF-8 was 17.93 ± 2.03 mV, and after loading GCV, the potential value becomes 25.97 ± 0.79 mV (Fig. 1j), which also indicated that GCV was loaded into ZIF-8, and the result was consistent with that confirmed in Fig. 1g. In addition, after further coating HA, the potential value directly changes from 25.97 ± 0.79 mV to − 9.63 ± 4.50 mV, because HA contains a large number of carboxyl groups as negatively charged substances. When the carboxyl group of HA is coordinated with Zn^{2+} in GCV@ZIF-8, its negative charge cancels out the positive charge in GCV@ZIF-8. This also proved that GCV@ZIF-8 is successfully coated and consistent with those confirmed in Fig. 1c, f, and h.

Meanwhile, we tested the particle size of ZIF-8, GCV@ZIF-8 and HA/GCV@ZIF-8 to determine whether they were easy to enter cells and found that ZIF-8 was 209.5 nm. After loading GCV, the particle size changesd slightly and increased to 223.4 nm. After further coating of HA, the particle size increased to 237.7 nm (Fig. 1k). TGA curves of ZIF-8, GCV@ZIF-8 and HA/GCV@ZIF-8 are observed in Fig. 1l showing that when the temperature rises to about 600℃, the weight of ZIF-8 and GCV@ZIF-8 begins to decrease. This is due to the removal of the organic ligand (2-MIM) of ZIF-8 and the organic small molecule drug GCV loaded in ZIF-8 by heating. When the temperature is about 300℃, the weight of HA/GCV@ZIF-8 tends to decline, which is faster than that of GCV@ZIF-8, the reason is caused by the HA covering GCV@ZIF-8. All the above results indicated that HA/GCV@ZIF-8 was successfully prepared with the weak negative potential and suitable particle size for the endocytosis.

Analysis of GCV loading rate and release performance in vitro

ZIF-8 was often used as a drug carrier because of its pH response to decomposition. To explore whether HA/GCV@ZIF-8 can serve as a pH-responsive drug delivery system, we conducted in vitro experiments simulating the release of GCV in the tumor microenvironment in response to pH (Fig. 2a). The drug loading rates of GCV@ZIF-8 and HA/GCV@ZIF-8 were calculated by formula (1) to be 7.2% and 5.6%, respectively. It is worth noting that after further coating HA, the GCV loading rates did not change greatly. The 1.6% reduction of HA/GCV@ZIF-8 may be caused by the loss during washing centrifugation, which further proved that GCVwas loaded onto the carrier by encrusted inside ZIF-8. If GCV was loaded only on the outer surface, it is easy to be washed out, resulting in a great change in drug loading rate.

Next, we futher detect the cumulative release rate of GCV by formula (2) in vitro. When pH was 7.4, it reached about 26.91% and stabilized at 12 h (Fig. 2b), which proved that HA/GCV@ZIF-8 can be stable and drugs do not leak prematurely in the blood circulation, which has the effect of improving drug utilization rate. When pH was 5.0, it reached to 60.67% at 12 h, and 65.87% at 18 h (Fig. 2b). The GCV release trend was higher than it at pH 7.4, which may be mainly due to the release of GCV caused by the decomposition of ZIF-8 in a slightly acidic environment. In order to more intuitively monitor the drug release ability of HA/GCV@ZIF-8, it was incubated in PBS solution (pH = 5.0) for different times and its morphology changes were observed (Fig. 2c). With the increase of incubation time, the shape of HA/GCV@ZIF-8 gradually changed irregularly after 6 h, and it was acid-lyzed into fragments after 12 h, but some of it was still not completely acid-lyzed, and basically all of it was acid-lyzed after 24 h, and its acid-lyzing trend was basically consistent with the cumulative drug release results in Fig. 2b. All these results suggest that HA/GCV@ZIF-8 can be used as a pH-responsive drug delivery system, which has the potential to release drugs at the tumor site for anti-KSHV and eventually be eliminated through the kidney.

In vitro biosafety analysis

The emergence and development of nanomedicine delivery system is mainly for better use in vivo to play a specific function. The physiological environment of the human body is extremely complex, so it is very necessary to conduct biosafety analysis of

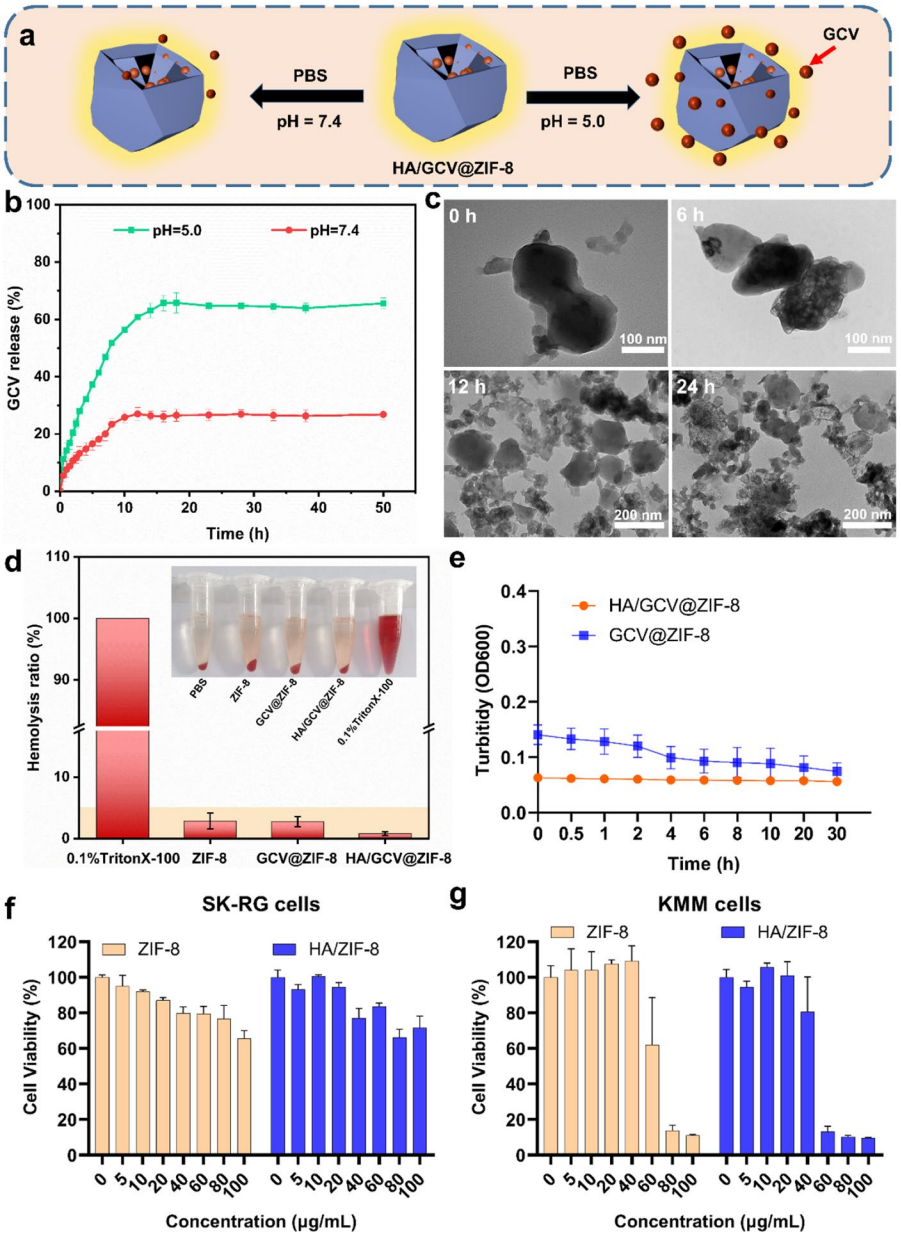

Fig. 2 Drug release properties of HA/GCV@ZIF-8, hemolysis rate, stability and empty cell toxicity. **a** Schematic diagram of HA/GCV@ZIF-8 hydrolyzed in PBS solution at pH = 7.4 and pH = 5.0, **b** cumulative release rate of GCV, and **c** TEM diagram of HA/GCV@ZIF-8 incubated in PBS solution at pH = 5.0 for 0 h, 6 h, 12 h, and 24 h. **d** Hemolysis rates and macroscopic hemolysis maps of ZIF-8, GCV@ZIF-8, HA/GCV@ZIF-8; **e** turbidity changes maps of GCV@ZIF-8 and HA/GCV@ZIF-8 in 50% FBS; **f**, **g** cell survival rate after incubation of empty carrier ZIF-8 and HA/ZIF-8 with KSHV-positive SK-RG and KMM cells at different concentrations for 48 h. Data are presented as mean ± SD ($n = 3$)

nanomaterials before entering the blood. Among them, the hemolysis rate after the interaction between the nanocore and the red blood cells in the blood is an important index to evaluate its biosafety. It can be intuitively seen in Fig. 2d that when the concentrations of ZIF-8, GCV@ZIF-8, and HA/GCV@ZIF-8 were 1 mg/mL, the

supernatant color as same as the negative control group (PBS). The red blood cells deposited at the bottom, and did not show the same hemolysis phenomenon as the positive control group (0.1% Triton-100). Their hemolysis rates were 2.88%, 2.76% and 0.83%, all within the safe range of hemolysis (< 5%). Compared with ZIF-8 and GCV@ZIF-8, HA/GCV@ZIF-8 has a lower hemolysis rate, indicating that the modification of HA can improve the blood compatibility of the material.

Nanocarriers are easy to interact with serum proteins in the blood vessel, and once the nanocarriers adsorb too much serum proteins, it is easy to cause cytotoxicity. Therefore, we tested the serum stability of drug-carrying nanocomplexes by detecting their turbidity changes in serum. When GCV@ZIF-8 was incubated with serum, the turbidity changed slightly within 30 h (Fig. 2e), while the absorbance of HA/GCV@ZIF-8 remained basically unchanged, which may be mainly due to the potential value of HA/GCV@ZIF-8 being − 9.63 ± 4.50 mV. Most of the serum proteins in the blood are also negative potentials, and adsorption between them is not easy, so that the turbidity is more stable.

To further verify the biosafety, we tested the cell survival rate after incubation with empty vectors for 48 h. There were less toxic to SK-RG cells when the concentration was about 80 μg/mL of ZIF-8 and 60 μg/mL of HA/ZIF-8 (Fig. 2f). For KMM cells (Fig. 2g), the concentrations of ZIF-8 and HA/ZIF-8 was near 40 μg/mL produced less toxicity. When the concentration was greater than 60 μg/mL, it will produce significant toxicity, but the concentration will not be used in practical applications. It can be concluded that

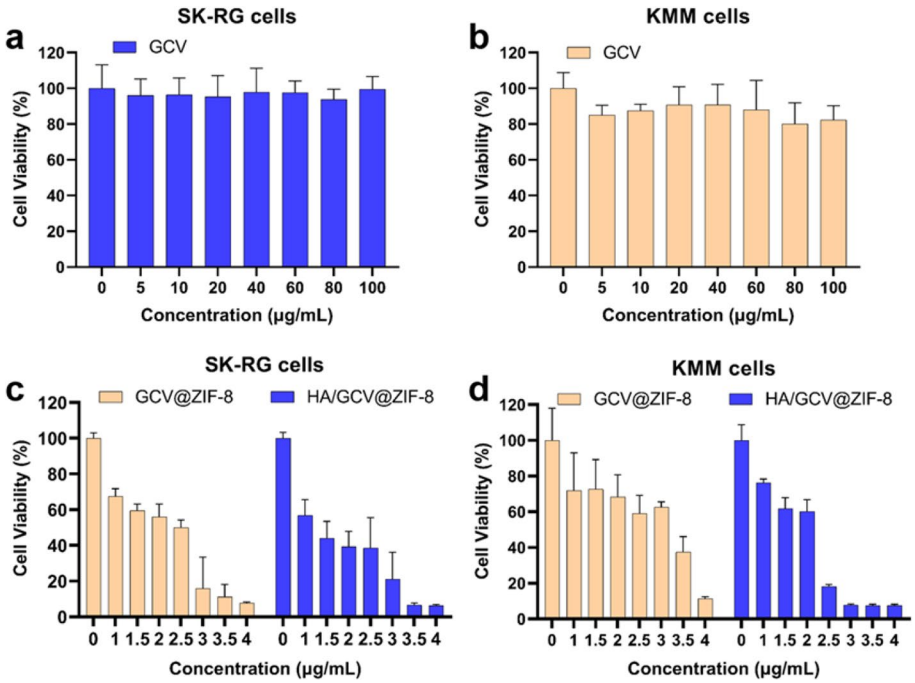

Fig. 3 Cytotoxicity. **a**, **b** Cell viability maps of GCV incubated with SK-RG and KMM cells at different concentrations for 48 h; **c**, **d** cell viability graphs of GCV@ZIF-8, HA/GCV@ZIF-8 incubated with SK-RG and KMM cells for 48 h (where the horizontal concentration was the concentration of GCV in GCV@ZIF-8 and HA/GCV@ZIF-8). Data are presented as mean ± SD ($n = 5$)

empty vector was cytocompatible. In summary, all the results proved that the nanocarriers have good biocompatibility and can be used for GCV delivery.

Toxicity analysis of the drug-carrying nanocomplex

To investigate the toxicity of nanocarriers on KSHV-positive cells, we seted up free GCV group, GCV@ZIF-8 group and HA/GCV@ZIF-8 group with targeted substances for experiments. First, we tested the cell survival rate of free GCV incubated with SK-RG cells and KMM cells at different concentrations for 48 h. When GCV concentrations ranged from 0 to 100 μg/mL, the survival rate of SK-RG cells still remained above 95% (Fig. 3a) and that of KMM cells remained at 80% (Fig. 3b). This suggests that free GCV itself has a low transmembrane capacity and is hard to enter the cell and play the role of resist KSHV. Then, we investigated the cell survival rates of GCV@ZIF-8 (Fig. 3c and d) and HA/GCV@ZIF-8 (Fig. 3c and d) incubated with SK-RG cells and KMM cells for 48 h. In both GCV@ZIF-8 group and HA/GCV@ZIF-8 group, the cytotoxicity increased with the increase of concentration, showing obvious drug concentration dependence. Among them, the IC_{50} of SK-RG and KMM cells in GCV@ZIF-8 was 1.813 μg/mL and 2.789 μg/mL, respectively. And in the HA/GCV@ZIF-8 group was 1.304 μg/mL and 1.410 μg/mL, respectively (Table S2). This also suggested that GCV can produced significant therapeutic effects at a very low concentration if it can enter into cells. Meanwhile, it is worth noting that under the same concentration condition, the cytotoxicity of HA/GCV@ZIF-8 group with targeted substance to SK-RG and KMM cells is higher than that of GCV@ZIF-8, indicating that HA modification not only increase the targeted delivery

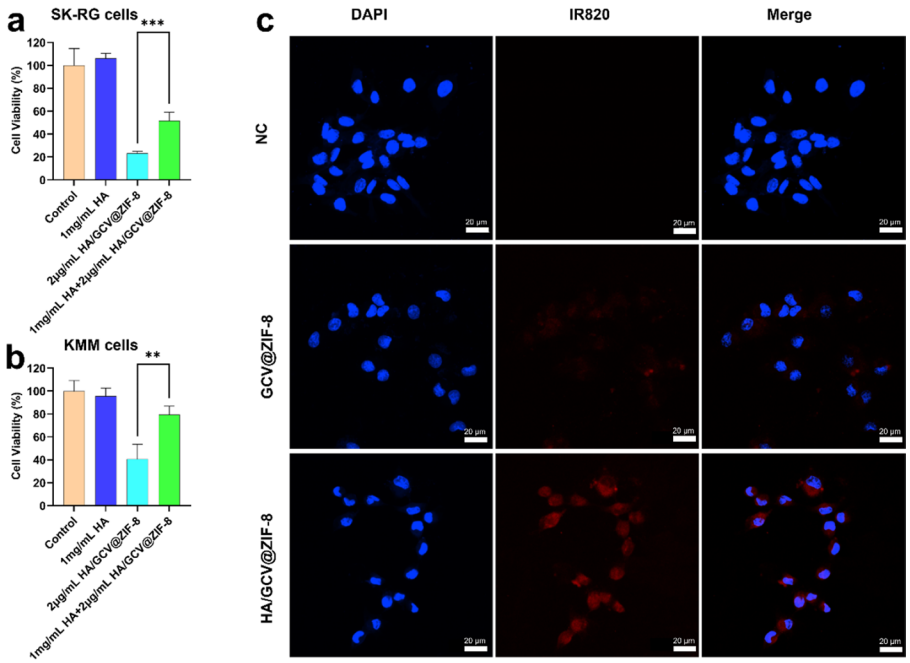

Fig. 4 HA competition experiment and cellular uptake in vitro. **a**, **b** Cell survival rate of SK-RG and KMM cells treated with mixture of free HA, HA/GCV@ZIF-8, HA/GCV@ZIF-8 + free HA group for 48 h. **c** CLSM images of KMM cells after treating with GCV@ZIF-8, HA/GCV@ZIF-8 for 4 h (scale bar = 20 μm). Data are presented as mean ± SD ($n = 5$), *$p < 0.05$, **$p < 0.01$, ***$p < 0.001$

effect of drug-carrying nanocomplex, but also enable GCV to play its curative effect with the least dose.

In vitro targeting analysis and cell uptake of the drug-carrying nanocomplex

Tumor cell membranes can overexpress CD44 receptors, which can bind to HA specifically, and then target tumor cells through CD44 receptor-mediated endocytosis (Figure S3a). So we detect the expression of CD44 protein in SK-RG and KMM cells by western blot, and found that these cells can express CD44 protein (Figure S3b). In addition, HA competition experiment was used to futher verify the targeting ability of HA/GCV@ZIF-8. Free HA has no killing effect on SK-RG and KMM cells, while HA/GCV@ZIF-8 has killing effect on these two cells (Fig. 4a and b). However, when HA/GCV@ZIF-8 is incubated with free HA, the cell activity is enhanced. This indicates that free HA can bind to the CD44 receptor on the cell surface more quickly, occupying the active site of the receptor, resulting in weakened targeting of HA/GCV@ZIF-8. This result is consistent with the results of cytotoxicity experiments, and proves that HA indeed plays a targeting role.

To further investigate the cellular uptake ability, KMM cells were treated with GCV@ZIF-8 and HA/GCV@ZIF-8 for 4 h, and then observed by CLSM. It can be clearly that GCV@ZIF-8 showed weak red fluorescence intensity distributed around the nucleus, while HA/GCV@ZIF-8 group had a stronger intensity (Fig. 4c and Supplement S2). This proved that HA-modified can be easier to deliver GCV.

Effect of HA/GCV@ZIF-8 on the cell proliferation, migration, and wound healing

The effects of GCV, GCV@ZIF-8, HA/GCV@ZIF-8 on the proliferation of SK-RG and KMM cells shown that at day 2, compared with the blank control group, GCV, GCV@ZIF-8 and HA/GCV@ZIF-8 all inhibited the proliferation of SK-RG cells (Fig. 5a). Among them, HA/GCV@ZIF-8 had the best inhibitory effect on SK-RG cells proliferation. Essentially the same results were shown in KMM cells (Fig. 5b). In conclusion, the results suggest that HA/GCV@ZIF-8 can inhibit the proliferation of KSHV-positive SK-RG and KMM cells.

Cell migration is closely related to tumor metastasis, so inhibiting cell migration can effectively inhibit tumor progression. Transwell assay was used to evaluate the inhibitory effect of drug-loaded nanocomplexes in vitro (Fig. 6a). The number of KMM and

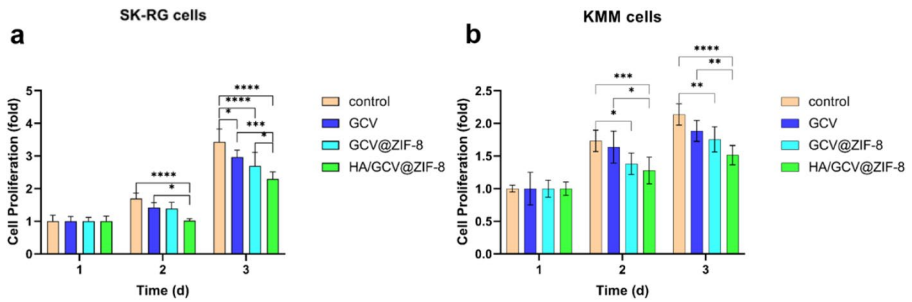

Fig. 5 Cell proliferation. **a** Effect of GCV, GCV@ZIF-8, HA/GCV@ZIF-8 on the proliferation of SK-RG cells and **b** KMM cells. Data are presented as mean ± SD ($n = 5$), *$p < 0.05$, **$p < 0.01$, ***$p < 0.001$, ****$p < 0.0001$

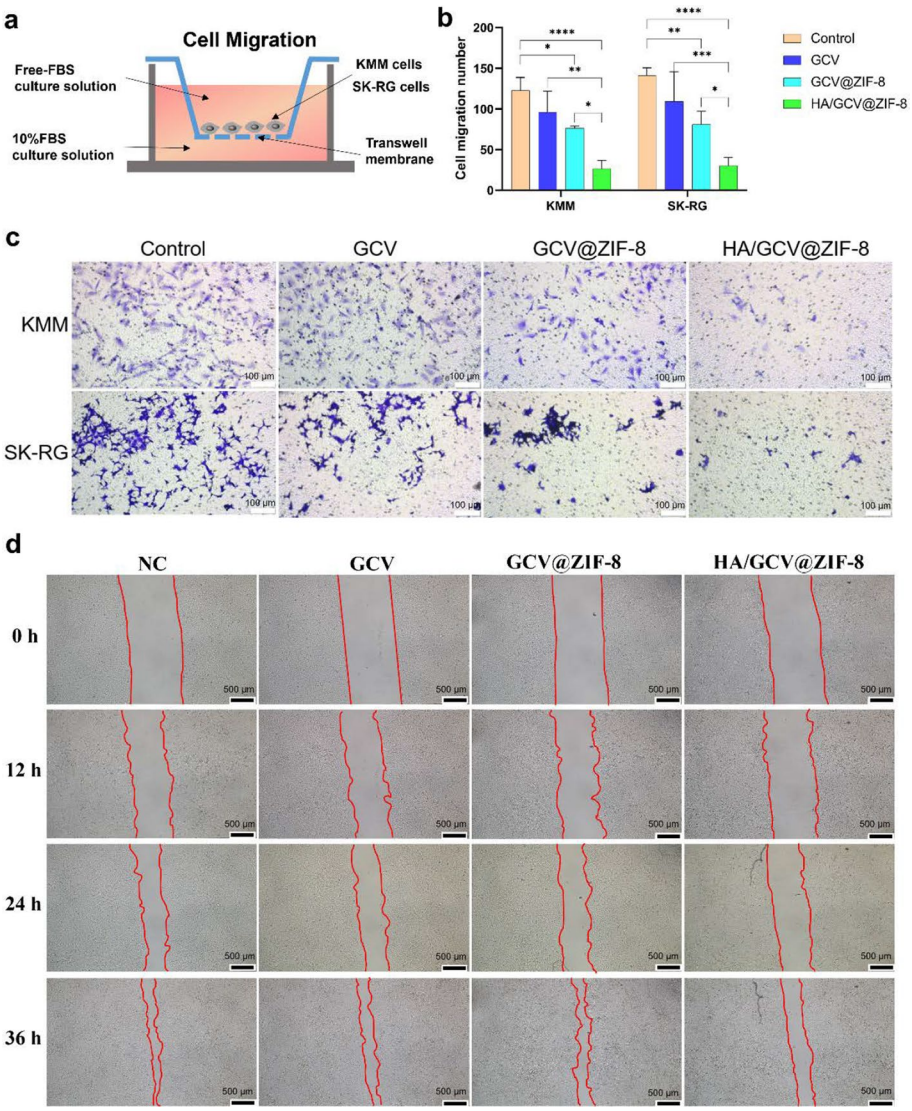

Fig. 6 Cell migration and wound healing. **a** Transwell experiment diagram, **b** quantitative cell migration diagram, **c** cell migration microscope (scale bar = 100 μm) of KMM and SK-RG cells treated with GCV, GCV@ZIF-8 and HA/GCV@ZIF-8 for 36 h. **d** Cellular wound healing microscopy (scale bar = 500 μm). Data are presented as mean ± SD ($n = 3$), *$p < 0.05$, **$p < 0.01$, ***$p < 0.001$, ****$p < 0.0001$

SK-RG cells in the free GCV group, GCV@ZIF-8 group, and HA/GCV@ZIF-8 group treated for 36 h was reduced than the control group, demonstrating a significant inhibitory effect, and the inhibitory effect of HA/GCV@ZIF-8 group was stronger than that in other groups (Fig. 6c). It can also be visually seen from the quantitative analysis results that the number of cell migration after treatment of KMM and SK-RG cells in the HA/GCV@ZIF-8 group is the smallest (Fig. 6b), which also indicates that the modification of HA increases the uptake of drugs by cells, thus playing a better role in inhibiting cell migration. We also evaluate the migration ability of HA/GCV@ZIF-8 by wound healing

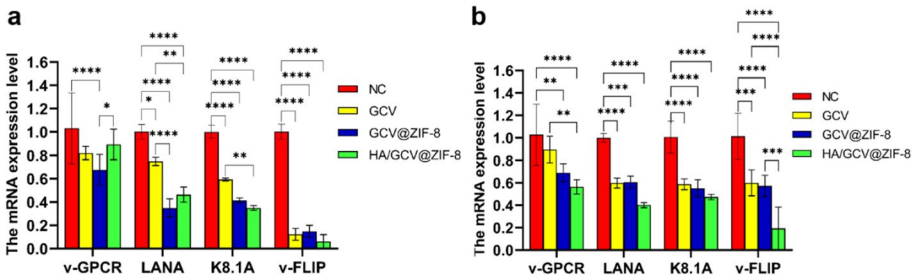

Fig. 7 Expression of KSHV-related genes was detected by RT-PCR. **a** mRNA expression levels of KSHV-related genes in SK-RG cells; and **b** KMM cells treated with GCV, GCV@ZIF-8, HA/GCV@ZIF-8. Data are presented as mean ± SD ($n = 3$), *$p < 0.05$, **$p < 0.01$, ***$p < 0.001$, ****$p < 0.0001$

assay and found that scratches in the control group gradually narrowed, and GCV group was similar to the control group, but GCV@ZIF-8 showed certain inhibitory effect on wound healing of KMM cells, it was not very obvious (Fig. 6d). Scratches in HA/GCV@ZIF-8 group converged more slowly over time than those in other groups, showing obvious inhibition of wound healing. In general, HA/GCV@ZIF-8 can inhibit the migration ability of KMM cells.

RT-PCR detected the level of KSHV-related genes

Like other herpesviruses, after infecting cells, KSHV exists in two different states to encode and express different disease-causing genes (Chen et al. 2019). So we further detected the level of KSHV latent genes latency-associated nuclear antigen(LANA) 2019, viral FLICE inhibitory protein (v-FLIP) and viral G protein coupled receptor (v-GPCR), K8.1A to verify whether HA/GCV@ZIF-8 can effectively inhibit KSHV expression. After treatment with HA/GCV@ZIF-8, the mRNA expression levels of lytic gene v-GPCR, K8.1A and latent gene LANA and v-FLIP were great decrease (Fig. 7a and b), which indicted that HA/GCV@ZIF-8 can inhibit KSHV replication and play the role of antiviral function effectively.

In vivo fluorescence imaging and anti-tumor effect

Fluorescence imaging is a method of detecting drug distribution in the body, so we used IR820 to monitor the distribution of HA/GCV@IR820@ZIF-8 in vivo. Firstly, nude mice were injected with KMM cells to construct tumor model, and then GCV@IR820@ZIF-8 and HA/GCV@IR820@ZIF-8 were injected peritumoral to observe the distribution, as shown in Fig. 8a, after injection of 1 h, we could see the fluorescence and the intensity was strongest after 8 h at the tumor site. After 24 h, the fluorescence intensity of HA/GCV@IR820@ZIF-8 was still higher, indicating that the active targeting of the tumor site mediated by HA enables the enrichment of drug-carrying nanocomplex. To further illustrate these results, we continued to observe the fluorescence signals of the drug-carrying nanocomplex in anatomical organs (heart, liver, spleen, lung, kidney) and tumors, the fluorescence intensity of HA/GCV@IR820@ZIF-8 in tumors was higher than that

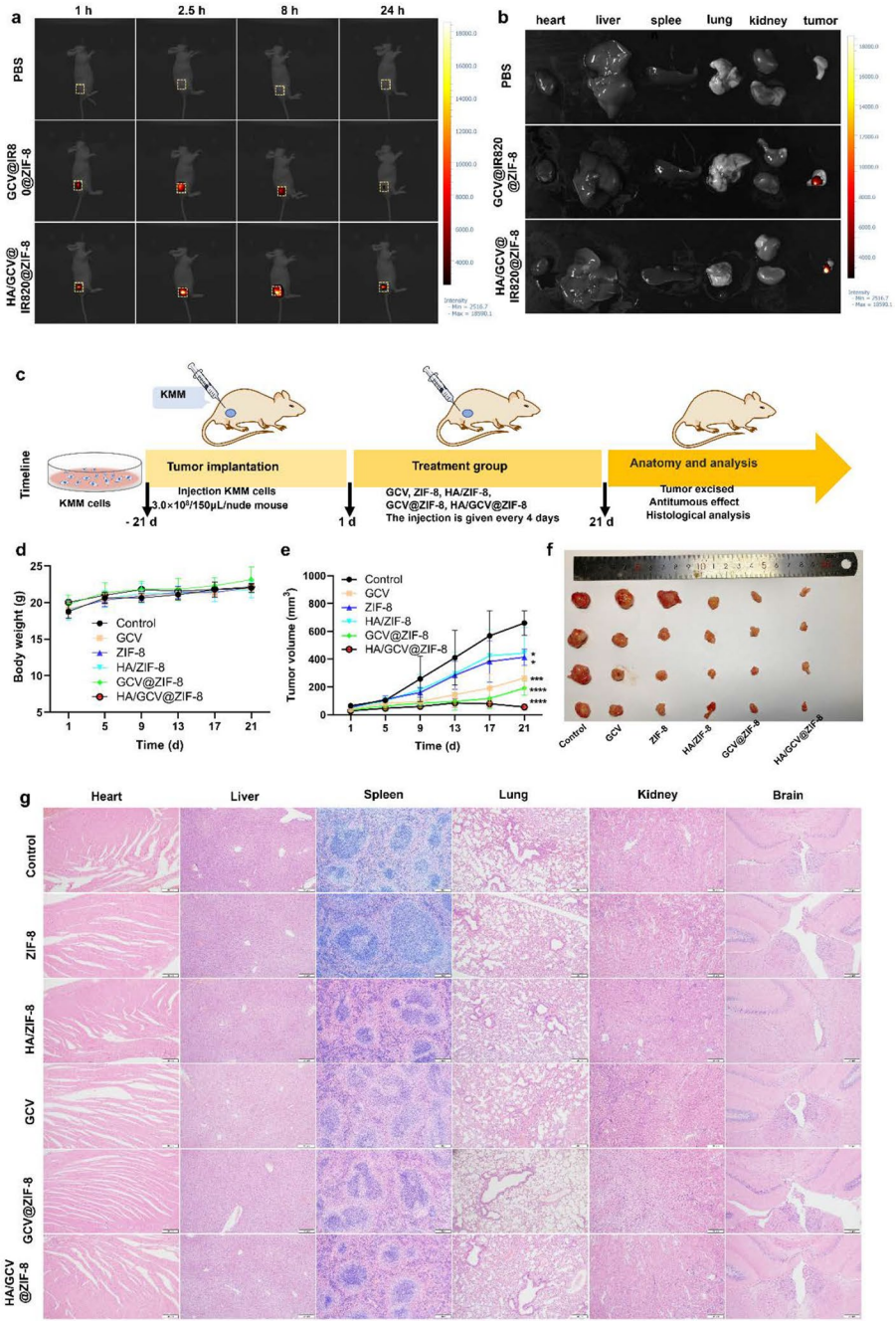

Fig. 8 In vivo imaging and evaluation of anti-tumor effect. **a** Distribution of GCV@IR820@ZIF-8 and HA/GCV@IR820@ZIF-8 at different times; **b** fluorescence imaging of related organs and tumors after 24 h. **c** Schematic diagram of experimental design ($n=4$); **d** weight change of nude mice over time; **e** tumor size change over time (*$P<0.05$;***$P<0.001$; ****$P<0.0001$); **f** tumor size of nude mice in each group after 21 days of treatment. **g** HE staining of different organs (heart, liver, spleen, lung, kidney and brain) in each group (scale: 200 μm). Data are presented as mean ± SD ($n=4$)

of GCV@IR820@ZIF-8 (Fig. 8b). These results indicate that HA-modified drug-carrying nanocomplex can better enrich in tumor sites.

We further evaluated the therapeutic effect in vivo as shown in Fig. 8c. The weight and tumor volume of nude mice were recorded during treatment to evaluate the safety and anti-tumor effect. After treatment of nude mice in each group, the body weight did not decrease (Fig. 8d), indicating that there was no obvious toxicity in all sample groups. The curve of tumor volume size is shown in Fig. 8e, compared with the blank control group, all treatment groups had different degrees of tumor inhibition within 21 days, among which the HA/GCV@ZIF-8 group had the best inhibitory effect on tumor growth, which was mainly attributed to the enhanced enrichment of GCV at the tumor site by HA-modified drug-carrying nanocomplex, followed was GCV@ZIF-8 group, which had a better inhibitory effect than free GCV group. The tumor tissue images of each group after 21 days in Fig. 8f also visually showed anti-tumor effects, which were basically consistent with the results in Fig. 8e, HA/GCV@ZIF-8 showed good anti-tumor effects. In addition, after the end of the experiment, major organs of nude mice were collected for tissue sections and HE staining showing no obvious physiological abnormalities in Fig. 8g, which also proved that the empty carrier and drug-carrying nanocomplex had good biocompatibility.

Conclusions

In conclusion, a nano-drug delivery system loaded with antiviral drugs was successfully prepared for the treatment of KSHV-associated malignancies by "one-pot method". The HA/GCV@ZIF-8 potential was -9.63 ± 4.50 mV, which had good stability in serum for 30 h. Under the simulated tumor slightly acidic condition, the GCV's release rate of HA/GCV@ZIF-8 reached to 65.87%, which proved its pH response to drug release characteristics. ZIF-8 uses its biological properties to support GCV and improve the transmembrane ability. Hemolysis experiment, cytotoxicity experiment, in vitro HA competition and cell uptake experiment all showed that HA modification not only reduce the hemolysis rate and improve the stability of drug-carrying nanocomplex, but also increase the uptake of cells, reduce the toxic side effects of GCV. Further cell experiments showed that drug-carrying nanocomplex could inhibit the proliferation, cell migration, and reduce the level of KSHV-relate genes, thus playing an effective anti-KSHV role. The most important thing is that the drug-carrying nanocomplex also showed better inhibitory effect on tumor growth in nude mice. These findings may provide potential application value for the treatment of KSHV-related malignancies.

Supplementary Information

The online version contains supplementary material available at https://doi.org/10.1186/s12645-024-00303-0.

Additional file 1: Figure S1. **a** Ultraviolet–visible full-wavelength scan of GCV, **b** Standard curve of GCV. Table S1. The sequences of primers. Table S2. IC_{50} values of SK-RG and KMM cells treated by GCV@ZIF-8, HA/GCV@ZIF-8. Figure S2. **a**, **b** Cell viability graphs of GCV@ZIF-8 incubated with SK-RG and KMM cells for 48 h (where the horizontal concentration was the concentration of GCV in GCV@ZIF-8). Data are presented as mean ± SD ($n = 5$). Figure S3. **a** Specific binding diagram of HA and CD44 receptor, **b** strip diagram of CD44 protein expression in SK-RG and KMM cells.

Acknowledgements
Not applicable.

Author contributions
All authors contributed to the writing of this manuscript, and all contributors approved the final version of the manuscript. Fangling Li: Writing – original draft, Validation, Investigation, Formal analysis, Conceptualization, Funding acquisition. Chengjing Liu: Data curation, Formal analysis, Writing – original draft. Wenyi Gu: Data curation, Methodology. Qianhe Xu: Investigation, Methodology. Dongmei Li: Conceptualization, Funding acquisition, Methodology, Project administration, Validation, Writing –review & editing. Dongdong Cao: Conceptualization, Funding acquisition, Methodology, Project administration, Writing –review & editing. Zhiyong Liu: Project administration, Resources, Supervision.

Funding
We are grateful for the financial support by the Xinjiang Science and Technology Cooperation Project [Grant no. 2022BC002], International Cooperation Program of Shihezi University [Grant no. GJHZ202102] and National Natural Science Foundation of China [Grant no. 32460038 and 81760362], Shihezi University basic research project [Grant no. PYZK202410], Shihezi University innovative training project [Grant no. 202410759078].

Availability of data and materials
No datasets were generated or analysed during the current study.

Declarations

Ethics approval and consent to participate
The animal experiments were approved by the Ethics Committee of Shihezi University.

Consent for publication
Not applicable.

Competing interests
The authors declare no competing interests.

Received: 22 August 2024 Accepted: 20 December 2024
Published online: 04 January 2025

References

Ablashi DV, Chatlynne LG, Whitman JE Jr, Cesarman E (2002) Spectrum of Kaposi's sarcoma-associated herpesvirus, or human herpesvirus 8, diseases. Clin Microbiol Rev 15(3):439–464. https://doi.org/10.1128/cmr.15.3.439-464.2002
Al-Badr AA, Ajarim TDS (2018) Ganciclovir. Prof Drug Subst Excip Relat Methodol 43:1–208. https://doi.org/10.1016/bs.podrm.2017.12.001
Carbone A, Vaccher E, Gloghini A (2022) Hematologic cancers in individuals infected by HIV. Blood 139(7):995–1012. https://doi.org/10.1182/blood.2020005469
Casper C, Krantz EM, Corey L, Kuntz SR, Wang J, Selke S, Hamilton S, Huang ML, Wald A (2008) Valganciclovir for suppression of human herpesvirus-8 replication: a randomized, double-blind, placebo-controlled, crossover trial. J Infect Dis 198(1):23–30. https://doi.org/10.1086/588820
Chang HH, Ganem D (2013) A unique herpesviral transcriptional program in KSHV-infected lymphatic endothelial cells leads to mTORC1 activation and rapamycin sensitivity. Cell Host Microbe 13(4):429–440. https://doi.org/10.1016/j.chom.2013.03.009
Chen J, Dai Lu, Goldstein A, Zhang H, Wei Tang J, Forrest C, Post SR, Chen X, Qin Z (2019) Identification of new antiviral agents against Kaposi's sarcoma-associated herpesvirus (KSHV) by high-throughput drug screening reveals the role of histamine-related signaling in promoting viral lytic reactivation. PLoS Pathog. https://doi.org/10.1371/journal.ppat.1008156
Chen J, Zhang H, Chen X (2020) Pemetrexed inhibits Kaposi's sarcoma-associated herpesvirus replication through blocking dTMP synthesis. Antiviral Res 180:104825. https://doi.org/10.1016/j.antiviral.2020.104825
Chou S (2021) Opposite effects of cytomegalovirus UL54 exonuclease domain mutations on acyclovir and cidofovir susceptibility. Antiviral Res 195:105181. https://doi.org/10.1016/j.antiviral.2021.105181
Coen N, Duraffour S, Snoeck R, Andrei G (2014) KSHV targeted therapy: an update on inhibitors of viral lytic replication. Viruses 6(11):4731–4759. https://doi.org/10.3390/v6114731
Delyon J, Rabate C, Euvrard S, Harwood CA, Proby C, Güleç AT, Seçkin D, Del Marmol V, Bouwes-Bavinck JN, Ferrándiz-Pulido C, Ocampo MA, Barete S, Legendre C, Francès C, Porcher R, Lebbe C (2019) Management of Kaposi sarcoma after solid organ transplantation: a European retrospective study. J Am Acad Dermatol 81(2):448–455. https://doi.org/10.1016/j.jaad.2019.03.028
Ding M, Liu W, Gref R (2022) Nanoscale MOFs: from synthesis to drug delivery and theranostics applications. Adv Drug Deliv Rev. https://doi.org/10.1016/j.addr.2022.114496
Fang H, Yan HHN, Bilardi RA, Flensburg C, Yang H, Barbour JA, Siu HC, Turski M, Chew E, Xu Z, Lam ST, Sharma R, Xu M, Li J, Ip HW, Cheung CYM, Huen MSY, Sweet-Cordero EA, Majewski IJ, Leung SY, Wong JWH (2022) Ganciclovir-induced mutations are present in a diverse spectrum of post-transplant malignancies. Genome Med 14(1):124. https://doi.org/10.1186/s13073-022-01131-w

Fangling Li, Cao Dongdong Gu, Wenyi CL, Zhongpeng Q, Zhiyong L, Dongmei Li, Xuhong G (2023) Delivery of miR-34a-5p by folic acid-modified β-cyclodextrin-grafted polyethylenimine copolymer nanocarriers to resist KSHV. ACS Appl Nano Mater. https://doi.org/10.1021/acsanm.3c02162
Feng S, Mao Y, Wang X, Zhou M, Hongyan Lu, Zhao Q, Wang S (2019) Triple stimuli-responsive ZnO quantum dots-conjugated hollow mesoporous carbon nanoplatform for NIR-induced dual model antitumor therapy. J Colloid Interface Sci. https://doi.org/10.1016/j.jcis.2019.09.120
Ho SA, Slavin M, Roberts JA, Yong M (2021) Optimization of Ganciclovir use in allogeneic hematopoietic cell transplant recipients—the role of therapeutic drug monitoring. Expert Rev Anti Infect Ther 19(6):707–718. https://doi.org/10.1080/14787210.2021.1851193
Iftode N, Rădulescu MA, Aramă SŞ, Aramă V (2020) Update on Kaposi sarcoma-associated herpesvirus (KSHV or HHV8)—review. Rom J Intern Med 58(4):199–208. https://doi.org/10.2478/rjim-2020-0017
Jia T, Chenyi H, Yuanqi L, Wang Tianqi Yu, Mian HH, Weiwei Z, Wenxin H, Junqing W, Meiying Wu (2023) Metal-organic framework nanoshell structures: preparation and biomedical applications. Coord Chem Rev. https://doi.org/10.1016/j.ccr.2023.215211
Jin C-X, Shang H-B (2021) Synthetic methods, properties and controlling roles of synthetic parameters of zeolite imidazole framework-8: a review. J Solid State Chem. https://doi.org/10.1016/j.jssc.2021.122040
Journo G, Ahuja A, Dias-Polak D, Eran Y, Bergman R, Shamay M (2021) Global CpG DNA methylation footprint in Kaposi's sarcoma. Front Cell Infect Microbiol 11:666143. https://doi.org/10.3389/fcimb.2021.666143
Kesharwani P, Chadar R, Sheikh A, Rizg WY, Safhi AY (2022) CD44-targeted nanocarrier for cancer therapy. Front Pharmacol. https://doi.org/10.3389/fphar.2021.800481
Krell J, Stebbing J (2014) Broader implications of a stage-guided stratified therapeutic approach for AIDS-related Kaposi's sarcoma. J Clin Oncol 32(5):373–375. https://doi.org/10.1200/jco.2013.53.7126
Labo N, Miley W, Benson CA, Campbell TB, Whitby D (2015) Epidemiology of Kaposi's sarcoma-associated herpesvirus in HIV-1-infected US persons in the era of combination antiretroviral therapy. AIDS 29(10):1217–1225. https://doi.org/10.1097/qad.0000000000000682
Li F, Cao D, Gu W, Li D, Liu Z, Cui L (2024) Folate-targeted nanocarriers co-deliver ganciclovir and miR-34a-5p for combined anti-KSHV therapy. Int J Mol Sci. https://doi.org/10.3390/ijms25052932
Liu Z, Yan Z, Di Y, Yang S, Ning Y, Mao Y, Gao Y, Zhao Q, Wang S (2023) Current advances in metal–organic frameworks for cancer nanodynamic therapies. Coord Chem Rev. https://doi.org/10.1016/j.ccr.2023.215434
Lu J, Song L, Feng S, Wang K, Mao Y, Gao Y, Zhao Q, Wang S (2023) Nanozyme-mediated biocatalysis as a mitochondrial oxidative stress amplifier for tumor nanocatalytic immunotherapy. Chem Eng J. https://doi.org/10.1016/j.cej.2023.148270
Luo Z, Dai Y, Gao H (2019) Development and application of hyaluronic acid in tumor targeting drug delivery. Acta Pharm Sinica B. https://doi.org/10.1016/j.apsb.2019.06.004
Märtson AG, Edwina AE, Kim HY, Knoester M, Touw DJ, Sturkenboom MGG, Alffenaar JC (2022) Therapeutic drug monitoring of ganciclovir: where are we? Ther Drug Monit 44(1):138–147. https://doi.org/10.1097/ftd.0000000000000925
Merlin JPJ, Crous A, Abrahamse H (2023) Nano-phototherapy: favorable prospects for cancer treatment. Wiley Interdiscip Rev Nanomed Nanobiotechnol. https://doi.org/10.1002/wnan.1930
Morillo-Gutierrez B, Waugh S, Pickering A, Flood T, Emonts M (2017) Emerging (val)ganciclovir resistance during treatment of congenital CMV infection: a case report and review of the literature. BMC Pediatr 17(1):181. https://doi.org/10.1186/s12887-017-0933-6
Overchuk M, Zheng G (2018) Overcoming obstacles in the tumor microenvironment: recent advancements in nanoparticle delivery for cancer theranostics. Biomaterials 156:217–237. https://doi.org/10.1016/j.biomaterials.2017.10.024
Qin A, Chen S, Li S, Li Q, Huang X, Xia L, Lin Y, Shen A, Xiang AP, Zhang L (2022) Artificial stem cells mediated inflammation-tropic delivery of antiviral drugs for pneumonia treatment. J Nanobiotechnology 20(1):335. https://doi.org/10.1186/s12951-022-01547-x
Schulz TF (2000) Kaposi's sarcoma-associated herpesvirus (human herpesvirus 8): epidemiology and pathogenesis. J Antimicrob Chemother 45(3):15–27. https://doi.org/10.1093/jac/45.suppl_4.15
Serra M, Casas A, Toubarro D, Barros AN, Teixeira JA (2023) Microbial hyaluronic acid production: a review. Molecules. https://doi.org/10.3390/molecules28052084
Shi L, Jun Wu, Qiao X, Ha Y, Li Y, Peng C, Renbing Wu (2020) In situ biomimetic mineralization on ZIF-8 for smart drug delivery. ACS Biomater Sci Eng. https://doi.org/10.1021/acsbiomaterials.0c00935
Son M, Lee M, Sung GH, Lee T, Shin YS, Cho H, Lieberman PM, Kang H (2013) Bioactive activities of natural products against herpesvirus infection. J Microbiol 51(5):545–551. https://doi.org/10.1007/s12275-013-3450-9
Tao W, Zhao D, Li G, Li L, Li S, Ye H, Tian C, Yutong Lu, Li S, Sun Y, He Z, Sun J (2021) Artificial tumor microenvironment regulated by first hemorrhage for enhanced tumor targeting and then occlusion for synergistic bioactivation of hypoxia-sensitive platesomes. Acta Pharm Sinica B. https://doi.org/10.1016/j.apsb.2021.08.010
Valantin MA, Royston L, Hentzien M, Jary A, Makinson A, Veyri M, Ronot-Bregigeon S, Isnard S, Palich R, Routy JP (2022) Therapeutic perspectives in the systemic treatment of Kaposi's Sarcoma. Cancers (Basel). https://doi.org/10.3390/cancers14030484
Wu M-X, Yang Y-W (2017) Metal–organic framework (MOF)-based drug/cargo delivery and cancer therapy. Adv Mater. https://doi.org/10.1002/adma.201606134
Wu S, Wu Z, Xu H, Zhang J, Gu W, Tan X, Pan Z, Cao D, Li D, Yang L, Li D, Pan Y (2022) miR-34a-5p inhibits the malignant progression of KSHV-infected SH-SY5Y cells by targeting c-fos. PeerJ 10:e13233. https://doi.org/10.7717/peerj.13233
Xie H, Liu X, Huang Z, Liexi Xu, Bai R, He F, Wang M, Han L, Bao Z, Yuzhou Wu, Xie C, Gong Y (2022) Nanoscale zeolitic imidazolate framework (ZIF)-8 in cancer theranostics: current challenges and prospects. Cancers. https://doi.org/10.3390/cancers14163935
Yang F, Li S, Ji Q, Zhang H, Zhou M, Wang Y, Zhang S, Sun J, He Z, Luo C (2024) Modular prodrug-engineered oxygen nano-tank with outstanding nanoassembly performance, high oxygen loading, and closed-loop tumor hypoxia relief. Advanced Science. https://doi.org/10.1002/advs.202405583

Ye H, Wang K, Zhao J, Qi Lu, Wang M, Sun B, Shen Y, Liu H, Pané S, Chen X-Z, He Z, Sun J (2023) In situ sprayed nanovaccine suppressing exosomal PD-L1 by golgi apparatus disorganization for postsurgical melanoma immunotherapy. ACS Nano. https://doi.org/10.1021/acsnano.3c01733

Zhang SM, Rehling D, Jemth AS, Throup A, Landázuri N, Almlöf I, Göttmann M, Valerie NCK, Borhade SR, Wakchaure P, Page BDG, Desroses M, Homan EJ, Scobie M, Rudd SG, Berglund UW, Söderberg-Nauclér C, Stenmark P, Helleday T (2021) NUDT15-mediated hydrolysis limits the efficacy of anti-HCMV drug ganciclovir. Cell Chem Biol 28(12):1693-1702.e6. https://doi.org/10.1016/j.chembiol.2021.06.001

Ziqi Z, Ke Qiaomei Wu, Manni ZL, Ke J (2023) Pore space partition approach of ZIF-8 for pH responsive codelivery of ursolic acid and 5-fluorouracil. ACS Mater Lett. https://doi.org/10.1021/acsmaterialslett.2c01097

Publisher's Note